Nano Energy 38 (2017) 239–248

Contents lists available at ScienceDirect

Nano Energy

journal homepage: www.elsevier.com/locate/nanoen

Communication

Metallic and polar Co_9S_8 inlaid carbon hollow nanopolyhedra as efficient polysulfide mediator for lithium–sulfur batteries

Tao Chen[a], Lianbo Ma[a], Baorui Cheng[a], Renpeng Chen[a], Yi Hu[a], Guoyin Zhu[a], Yanrong Wang[a], Jia Liang[a], Zuoxiu Tie[a], Jie Liu[a,b], Zhong Jin[a,*]

[a] Key Laboratory of Mesoscopic Chemistry of MOE and Collaborative Innovation Center of Chemistry for Life Sciences, School of Chemistry and Chemical Engineering, Nanjing University, Nanjing, Jiangsu 210023, China
[b] Department of Chemistry, Duke University, Durham, NC 27708, USA

ARTICLE INFO

Keywords:
Lithium–sulfur batteries
Metallic and polar Co_9S_8
Hollow nanopolyhedra
Reaction kinetics
High areal capacity

ABSTRACT

Lithium–sulfur (Li–S) batteries are promising to replace current commercial Li–ion batteries due to the high energy density. Despite this, the poor cyclic stability induced by the shuttle effect of electrolyte-soluble intermediate polysulfides is one of the great obstacles for the application of Li–S batteries. To overcome this issue, here we report a self-template synthesis of metallic and polar Co_9S_8 nanocrystals inlaid carbon (Co_9S_8/C) hollow nanopolyhedra as an efficient sulfur host material. The Co_9S_8/C hollow nanopolyhedra with large inner space can ensure the loading mass of sulfur and buffer the volume expansion of Li_2S_x species during cycling; while the metallic and polar Co_9S_8/C shell offers synergetic spatial confinement and chemical binding to immobilize polysulfides and prevent the shutting effect. The Co_9S_8/C-S composite cathode exhibits high capacity and long cycle life with a low capacity decay of 0.041% per cycle over 1000 cycles at 2.0 C. When the areal sulfur content is as high as 3.0 mg cm^{-2}, the Co_9S_8/C-S cathode still maintains high cycling stability.

To satisfy the growing demand of portable devices and electric vehicles, high-energy-density rechargeable batteries are urgently required [1–6]. Lithium–sulfur (Li–S) batteries have become a promising candidate to replace current lithium-ion batteries, owing to the ultrahigh theoretical energy density (2600 Wh kg^{-1}) and the conspicuous advantages of sulfur, such as low cost, nontoxicity and natural abundance [7–12]. Nonetheless, the practical use of Li–S batteries faces several inherent obstacles. The intrinsically poor electrical conductivity of S_8 molecules often lead to a low utilization of active material, while the large volumetric variation during lithiation/delithiation processes causes the structural instability of electrode and short cycle life. Furthermore, the shuttle effect of intermediate polysulfides could result in low Coulombic efficiency and poor cycling stability of sulfur cathode [13–15]. To resolve these issues, extensive efforts have been dedicated to designing novel sulfur host materials, especially nanocarbons [16–25]. The porous and conductive carbon scaffolds can trap lithium polysulfides within nanopores through physical confinement. Unfortunately, the interaction between nonpolar carbon materials and sulfur species is normally too weak to suppress the diffusion of polysulfides over long-term cycling. Although heteroatom doping/substitution of carbon can provide some polar sites for the chemisorption of polysulfides [26–29], the binding energy is still low and the conductivity may decrease if the doping concentration is high.

To improve the confinement of intermediate polysulfides, inorganic polar materials (such as metal oxides [30–35], chalcogenides [36–39], nitrides [40], MXene, [41–43] etc.) have attracted great attention owing to the strong chemical affinity with sulfur species. However, the conductivity of polar host materials is generally low; the high charge transfer resistance may lead to sluggish interface redox reaction kinetics, thus decrease the sulfur utilization and rate capability. Moreover, different from nanocarbons, polar materials usually cannot offer large pore volume for the storage of sulfur species. Considering that the conductivity and pore volume of polar materials can be improved by the incorporation of carbon, there are anticipated benefits to developing hollow nanostructural inorganic/carbon composites as sulfur hosts that combine the advantages of nanocarbons and polar materials.

Here we report that metallic and polar Co_9S_8/carbon hollow nanopolyhedra can serve as an efficient sulfur host in Li-S batteries. With a self-templated synthesis method and a simple sulfidation process, hollow nanopolyhedra with carbon shells and inlaid polar Co_9S_8 nanocrystals were successfully prepared. The Co_9S_8/C hollow nanopolyhedra have several desirable features: (1) the hollow nanopolyhedra with large void space can accommodate high sulfur loading by

* Corresponding author.
E-mail address: zhongjin@nju.edu.cn (Z. Jin).

http://dx.doi.org/10.1016/j.nanoen.2017.05.064
Received 25 February 2017; Received in revised form 23 May 2017; Accepted 31 May 2017
Available online 02 June 2017

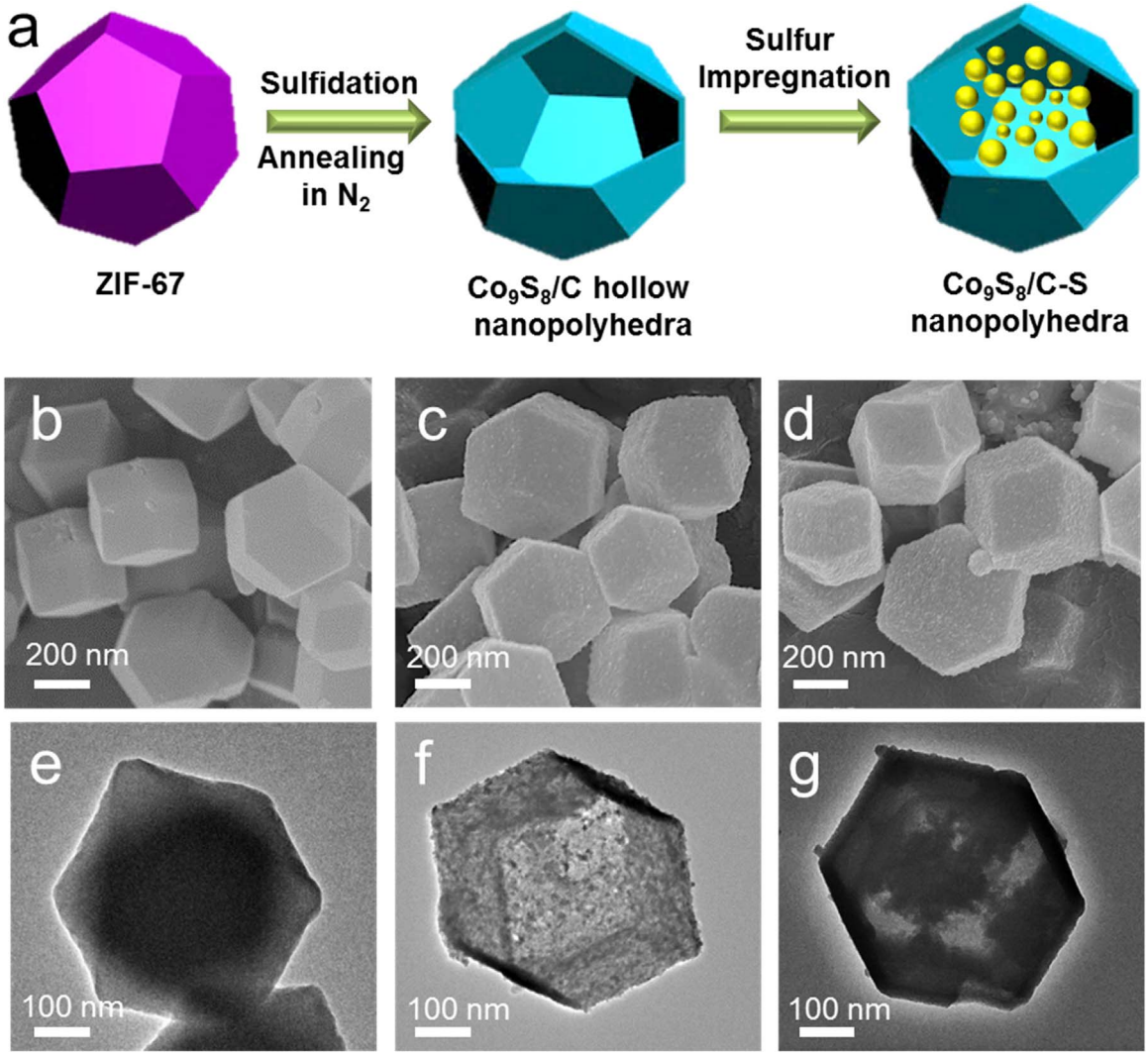

Fig. 1. (a) Schematic illustration of the synthesis process of Co_9S_8/C-S nanopolyhedra. SEM and TEM images of (b, e) ZIF-67 precursor nanopolyhedra, (c,f) Co_9S_8/C hollow nanopolyhedra and (d, g) Co_9S_8/C-S nanopolyhedra, respectively.

spatial confinement and buffer the volume variation; (2) the embedded Co_9S_8 nanocrystals are highly polar and quasi-metallic [44,45], it can strongly bind with polysulfides and restrict their outward diffusion (as evidenced by theoretical calculations and experiments); (3) polar Co_9S_8/C shells can also improve the redox reaction kinetics and rate capability; (4) the three-dimensional conductive and porous Co_9S_8/C outer shells are beneficial to facilitate Li^+ and electron transport. Compared to previously-reported sulfur composite cathodes, the Co_9S_8/C-S cathodes exhibit high reversible capacity, great rate performance and remarkable cycle stability even with high areal mass loading of sulfur (Table S1).

1. Results and discussion

The synthetic process of Co_9S_8/C nanopolyhedra and Co_9S_8/C-S composite is schematically shown in Fig. 1a. Firstly, monodispersed zeolitic imidazole framework-67 (ZIF-67) precursor nanopolyhedra were prepared via a reported precipitation method [46]. After subsequent sulfidation by thioacetamide (TAA) and annealing at 350 °C in N_2 atmosphere, Co_9S_8/C hollow nanopolyhedra were successfully obtained. Finally, sulfur was filled in Co_9S_8/C hollow nanopolyhedra via a melt-diffusion process to obtain Co_9S_8/C-S composite [47].

As shown in Fig. 1b-g, the morphology and structure of as-prepared samples were investigated by scanning electron microscopy (SEM) and transmission electron microscopy (TEM). The ZIF-67 precursor nanopolyhedra are uniform rhombic dodecahedra with smooth surface and an average size of ~500 nm (Fig. 1b,e). X-ray diffraction (XRD) pattern exhibits the sharp diffraction peaks of ZIF-67, indicating the high crystallinity (Fig. S1) [48–50]. The SEM image of Co_9S_8/C hollow nanopolyhedra (Fig. 1c) shows the external morphology and size of ZIF-67 are well maintained. Nevertheless, the TEM image reveals the formation of inner cavities (Figs. 1f and **2**a,b). The hollow structures were originated from the different diffusion rates of sulfur and cobalt species, with a mechanism similar to the Kirkendall effect (as described in Fig. S2) [51,52]. During the sulfidation process, the outward diffusion rate of cobalt ions from ZIF-67 was faster than the inward diffusion rate of S^{2-} ions from TAA, resulting the large internal cavities. High-resolution TEM images (Fig. 2c,d) exhibit the tiny Co_9S_8 nanoparticles homogenously distributed all over the shell of Co_9S_8/C hollow nanopolyhedra. The lattice distance in the inset of Fig. 2d is 0.29 nm, corresponding to the (311) plane of Co_9S_8 nanocrystals. The XRD pattern of Co_9S_8/C hollow nanopolyhedra (Fig. 2e) confirms the existence of cubic-phase Co_9S_8. Energy-dispersive X-ray spectroscopy (EDX) revealed a Co/S atomic ratio of 1.1, consistent with the stoichiometric ratio of Co_9S_8 (Fig. 2f). According to the EDX result, the atomic ratio of nitrogen in the Co_9S_8/C hollow nanopolyhedra is ~6.0%, mainly derived from the 2-methylimidazole ligands in the ZIF-67 precursor nanopolyhedra. The Raman spectrum of Co_9S_8/C hollow

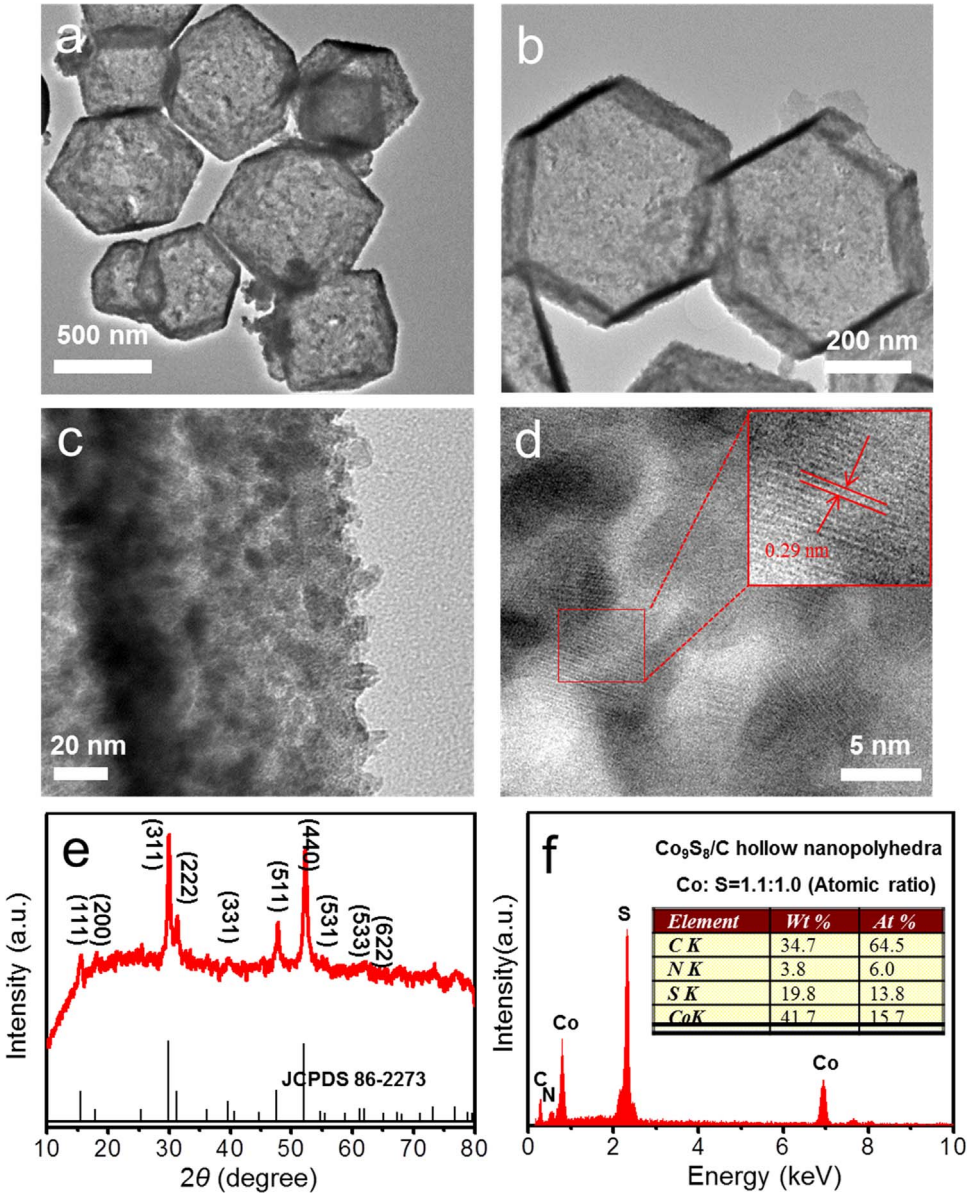

Fig. 2. TEM images of (a, b) Co_9S_8/C hollow nanopolyhedra, and (c) the shell of Co_9S_8/C hollow nanopolyhedra. (d) HRTEM image of Co_9S_8 nanocrystals embedded in the amorphous carbon network. (e) XRD pattern and (f) EDX spectrum of Co_9S_8/C hollow nanopolyhedra.

nanopolyhedra displays typical features of porous carbon, and the intensity ratio of D and G bands (I_D/I_G) is 1.1 (Fig. S3). After filling sulfur, the Co_9S_8/C-S nanopolyhedra still maintain high structural integrity, no sulfur particles are observed on the surface (Fig. 1d). TEM characterization (Fig. 1g) further confirms the successful encapsulation of sulfur inside hollow nanopolyhedra, and the remaining void space can effectively buffer the volume change during cycling. The EDX elemental mapping of Co_9S_8/C-S nanopolyhedra (Fig. S4) shows uniform distribution of C, Co and sulfur elements.

To investigate the chemisorption capability of Co_9S_8 nanocrystals towards lithium polysulfide species, the adsorption energies (E_a) between Co_9S_8 and different Li_2S_x species (or S_8 molecule) were calculated by the quantum density functional theory (QDFT) simulations [37,53,54]. The (202) planes of Co_9S_8 are chosen as the representative crystalline planes for the simulations, because the exposed atoms of (202) planes have a Co/S ratio of 5:4, which is very close to the stoichiometric ratio of Co/S in Co_9S_8. Fig. 3a shows the calculated E_a and the stable adsorption configurations of various sulfur-based species on the (202) planes of Co_9S_8 crystals. At the initial state, the E_a between S_8 molecule and Co_9S_8 is calculated to be −1.74 eV. As the lithiation process continues, the E_a of Li_2S_8, Li_2S_6, Li_2S_4, Li_2S_2 and Li_2S on the surface of Co_9S_8 (202) planes are −6.08, −4.03, −2.97, −4.52 and −5.51 eV, respectively. The chemical interaction of Li_2S_x species with Co_9S_8 is quite strong, mainly attributed to the coexistence of Co–S and Li–S bonds [37]. The binding energies of short-chain Li_2S_2/Li_2S species with Co_9S_8 are stronger than that of long-chain Li_2S_x species, resulted from the highly polar nature of both Li_2S_2/Li_2S species and Co_9S_8 nanocrystals. It could be speculated that the strong adsorption of short-chain Li_2S_2/Li_2S by Co_9S_8 can effectively suppress the shuttle effect, hence very conducive to the cyclic performance of the Li-S batteries based on Co_9S_8/C-S cathodes. To experimentally and visually compare the polysulfide adsorption ability of commercially-available activated carbon (AC) and Co_9S_8/C hollow nanopolyhedra, 50 mg of these samples were separately added into 2.0 mL of 0.2 wt% Li_2S_4 solution in a mixed solvent of dimethoxyethane/dioxolane (DME/DOL, v/v=1:1). As shown in Fig. 3b, the Li_2S_4 solution mixed with Co_9S_8/C hollow nanopolyhedra turned almost colorless after 120 min, while the Li_2S_4 solution mixed with AC were still yellow, confirming that the Co_9S_8/C hollow nanopolyhedra have much stronger adsorption capability for Li_2S_4 than common

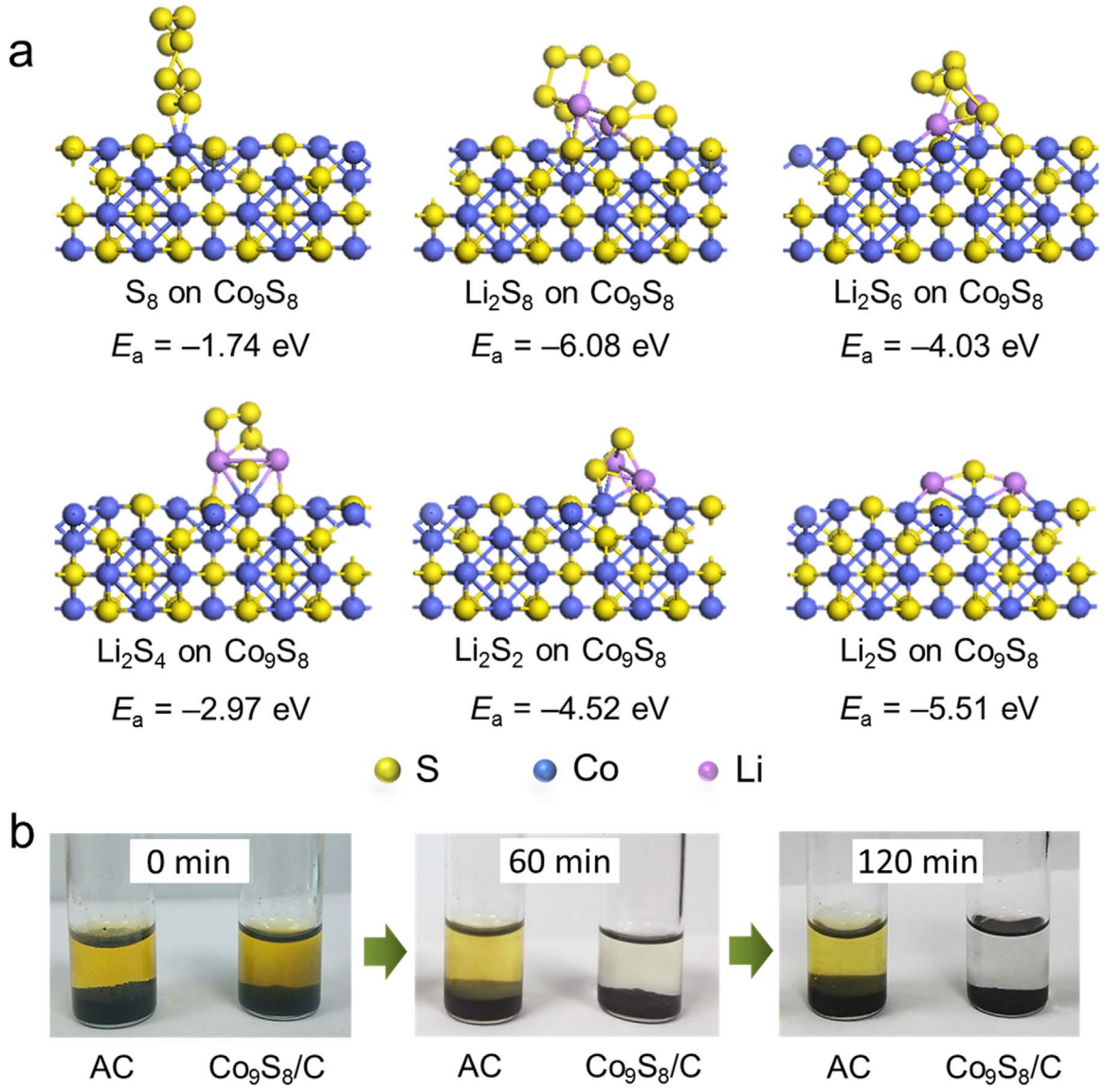

Fig. 3. (a) Calculated adsorption energies (E_a) of S_8 and Li_2S_x (x = 1, 2, 4, 6 or 8) species on the (202) planes of Co_9S_8 crystals. (b) Adsorption ability comparison of activated carbon (AC) and Co_9S_8/C hollow nanopolyhedra within the solution of Li_2S_4 as a representative polysulfide (in mixed DOL/DME solvents). The Li_2S_4 solution mixed with Co_9S_8/C hollow nanopolyhedra shows obvious discoloration in only 60 min, suggesting the high adsorption ability.

porous carbon. The adsorption experiment result and the above theoretical calculation indicate that the incorporation of metallic and polar Co_9S_8 nanocrystals in carbon nanostructures can greatly improve the confinement of intermediate polysulfides.

To examine the interaction between Li_2S_x and Co_9S_8, the X-ray photoelectron spectroscopy (XPS) analysis of the Co_9S_8/C hollow nanopolyhedra (Fig. S5) and the Co_9S_8/C-Li_2S_4 composite after adsorption experiment (Fig. S6) were also performed. For Co_9S_8/C hollow nanopolyhedra, two peaks at 778.3 and 780.9 eV correspond to Co atoms in the octahedral and tetrahedral sites of Co_9S_8, respectively (Fig. S5c) [52]; the peaks located at 161.3 and 162.5 eV correspond to S $2p_{3/2}$ and S $2p_{1/2}$ (Fig. S5d) [55]. The N 1s spectrum shows the co-existence of difference nitrogen species (pyridinic-N, pyrrolic-N and quaternary-N), which can offer more polar sites for immobilizing intermediate polysulfides (Fig. S5e). After the adsorption of Li_2S_4, the chemical interaction between Li_2S_4 and Co atoms in the Co_9S_8/C-Li_2S_4 composite is evidenced by the greatly decreased binding energies of Co $2p_{3/2}$ peaks at 777.5 and 778.5 eV (Fig. S6a). The terminal sulfur (S_T^{-1}) and bridging sulfur (S_B^{0}) species of Co_9S_8/C-Li_2S_4 composite are located at 161.8 and 163.0 eV (Fig. S6b), respectively, showing an overall +0.5 eV shift, which indicates the chemisorption of Li_2S_4 on the surface of Co_9S_8 [56]. The two other peaks at 167.2 and 168.5 eV were attributed to interaction of Li_2S_4 with the surface oxidized species of Co_9S_8 formed in air. Compared with Co_9S_8/C hollow nanopolyhedra, no obvious peak shifts were observed from the S 2p region of simply-mixed Li_2S_4 and Co_9S_8/C composite (Fig. S6c). Overall, the XPS analysis of Co_9S_8/C-Li_2S_4 composite confirms the chemical adsorption of lithium polysulfide on the surface of Co_9S_8 nanocrystals.

When used as cathode material for Li–S batteries, sulfur was filled into Co_9S_8/C hollow nanopolyhedra through a melt-diffusion method. Fig. 4a shows the XRD patterns of pure sulfur powder and Co_9S_8/C-S nanopolyhedra. The diffraction peaks of sulfur (JCPDS no. 08–0247) were also observed in the XRD spectrum of Co_9S_8/C-S nanopolyhedra, suggesting the presence of sulfur. The sulfur content of Co_9S_8/C-S nanopolyhedra was measured to be 77 wt% by thermogravimetric analysis (TGA) under N_2 atmosphere (Fig. 4b). To further investigate the porosity of Co_9S_8/C and Co_9S_8/C-S samples, nitrogen adsorption-desorption isotherms were measured. The Co_9S_8/C hollow nanopolyhedra show a type III isotherm with a hysteresis loop, showing a BET surface area of 187 $m^2 g^{-1}$ and a large specific pore volume of 1.8 m^3

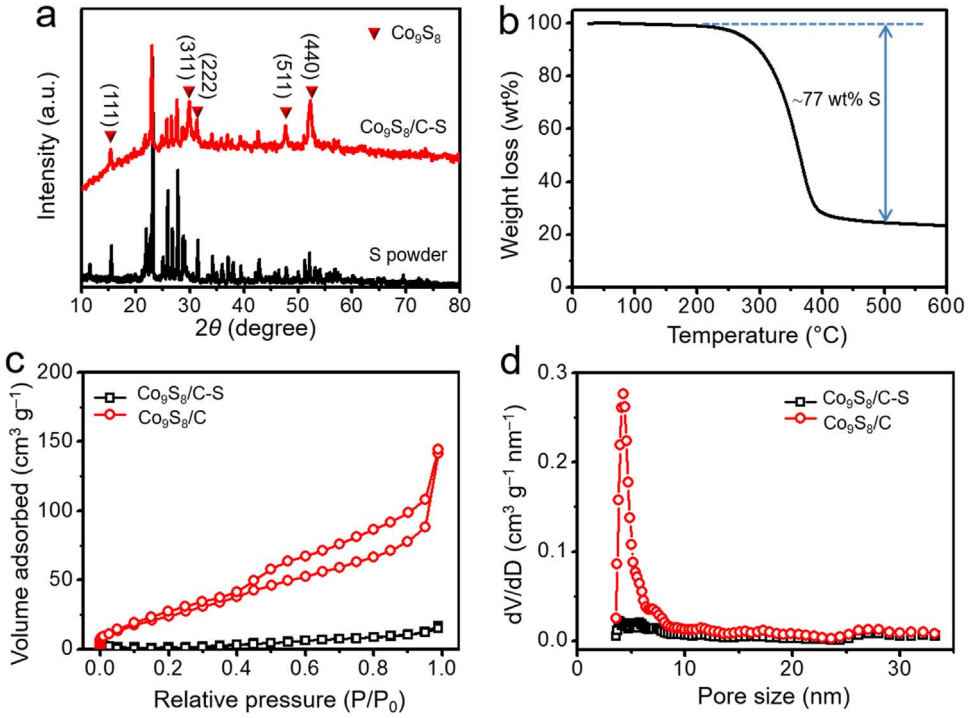

Fig. 4. (a) XRD patterns of sulfur powder and Co_9S_8/C-S nanopolyhedra. (b) TGA analysis of Co_9S_8/C-S nanopolyhedra. (c) Nitrogen adsorption-desorption isotherms and (d) corresponding pore size distributions of Co_9S_8/C hollow nanopolyhedra and Co_9S_8/C-S nanopolyhedra, respectively.

g^{-1} (Fig. 4c). According to the Barrett–Joyner–Halenda (BJH) method, the Co_9S_8/C hollow nanopolyhedra possess abundant mesopores centered at 4.2 nm (Fig. 4d). After sulfur impregnation, the surface area and pore volume of Co_9S_8/C-S nanopolyhedra sharply decreased to 34 $m^2 g^{-1}$ and 0.2 $m^3 g^{-1}$, indicating that sulfur was successfully filled into the interior cavities of Co_9S_8/C hollow nanopolyhedra.

To evaluate the performances of Co_9S_8/C-S nanopolyhedra for Li–S batteries, coin cells with Co_9S_8/C-S cathodes were fabricated. As control samples, Li-S batteries with sulfur-filled AC (AC-S) cathodes were also prepared. The sulfur content in AC-S composite was controlled to be ~78 wt%, almost identical to the Co_9S_8/C-S composite (Fig. S7). Fig. 5a shows the cyclic voltammetry (CV) curves of Co_9S_8/C-S cathode during the initial four cycles at 0.1 mV/s. In the 1st cycle, the cathodic peak at 2.26 V corresponds to the reduction of S_8 molecules to long-chain polysulfides (Li_2S_x, $4 \le x \le 8$), while the cathodic peak at ~2.03 V is ascribed to the reduction of long-chain Li_2S_x to short-chain Li_2S_2/Li_2S. The broad anodic peak at 2.37 V is assigned to the reverse conversion of short-chain Li_2S_2/Li_2S to S_8. After the activation of the first cycle, the CV curves of subsequent cycles exhibit sharper anodic/cathodic peaks with nearly-overlapped form, indicating the high reversibility of Co_9S_8/C-S cathode. The cycling performances of Co_9S_8/C-S and AC-S cathodes at a current density of 0.5 C was shown in Fig. 5b. The Co_9S_8/C-S cathode exhibits an initial discharge capacity of 1020 mAh g^{-1}, and still maintains a stable reversible capacity of 790 mAh g^{-1} after 200 cycles. In contrast, the AC-S cathode shows more rapid capacity decay and only delivers a discharge capacity of 490 mAh g^{-1} after 200 cycles, much inferior to the Co_9S_8/C-S cathode. Moreover, the Co_9S_8/C-S cathode exhibits a Coulombic efficiency (over 99%) higher than AC-S cathode (~95%), suggesting that the shuttle effect during cycling is effectively alleviated in Co_9S_8/C-S cathode. To compare the polysulfide adsorption capability after long-term cycling, the Co_9S_8/C-S and AC-S electrodes after cycling for 200 times were separately immersed into the mixed DOL/DME solvent (Fig. S8). The solution soaked with Co_9S_8/C-S electrode shows very light yellow color, indicating that only a trace amount of sulfur species is dissolved in electrolyte, and most of sulfur are still preserved inside the electrode owing to the effective confinement and adsorption of Co_9S_8/C hollow nanopolyhedra. In contrast, the DOL/DME solution soaked with AC-S electrode quickly changed to bright yellow. This result further confirms the outstanding polysulfide chemisorption capability of Co_9S_8/C hollow nanopolyhedra, which plays a decisive role to its superior cycling performance.

The rate performances of Co_9S_8/C-S and AC-S cathodes were investigated by cycling at various current rates from 0.2 to 3.0 C (Fig. 5c). The Co_9S_8/C-S cathode reached a high discharge capacity of ~1160 mAh g^{-1} at 0.2 C. When cycled stepwise at 0.5, 1.0, 2.0 and 3.0 C, the Co_9S_8/C-S cathode still delivered high reversible capacities of ca. 1080, 940, 880 and 690 mAh g^{-1}, respectively, indicting the high rate capability and fast reaction kinetics. When the current rate decreased back to 0.2 C again, 95% of the original specific capacity was recovered, suggesting the high stability of the Co_9S_8/C-S cathode. In contrast, the AC-S cathode suffered from rapid capacity decay at the same stepwise rates, showing discharge capacities of 880, 780, 650, 500 and 130 mAh g^{-1} at 0.2, 0.5, 1.0, 2.0 and 3.0 C, respectively. These results reveal that the incorporation of Co_9S_8 nanocrystals can also greatly enhance the reaction kinetics of polysulfide redox reactions, thus improve the rate capability of Li-S batteries.

To examine the long-term cycling stability of Co_9S_8/C-S cathode, fresh cells were firstly activated at 0.2 C for 5 cycles and then cycled at 2.0 C for 1000 cycles (Fig. 5e). After the activation process, the Co_9S_8/C-S cathode delivered a reversible capacity of 950 mAh g^{-1} at 2.0 C. During the initial 300 cycles, the discharge capacity of Co_9S_8/C-S cathode decreased to 795 mAh g^{-1}, corresponding to a capacity retention of 83.7%. In the following 400 cycles, the discharge capacity decreased gradually to a reversible value of 655 mAh g^{-1} with a capacity retention of 82.4%. After 1000 cycles, Co_9S_8/C-S cathodes still maintain a discharge capacity of 560 mAh g^{-1}. The capacity decay is only 0.041% per cycle and the Coulombic efficiency is ~99% throughout the whole process. Fig. S9 presents the electrochemical impedance spectrum (EIS) of Co_9S_8/C-S cathodes. The difference of charge-transfer resistance (R_{ct}) between fresh cell and after 200 cycles at 0.5 C is very small, suggesting the high cycling stability. To distinguish the capacity contributed by Co_9S_8/C host, the lithium storage behaviors of Co_9S_8/C hollow nanopolyhedra within the potential range of 1.7–

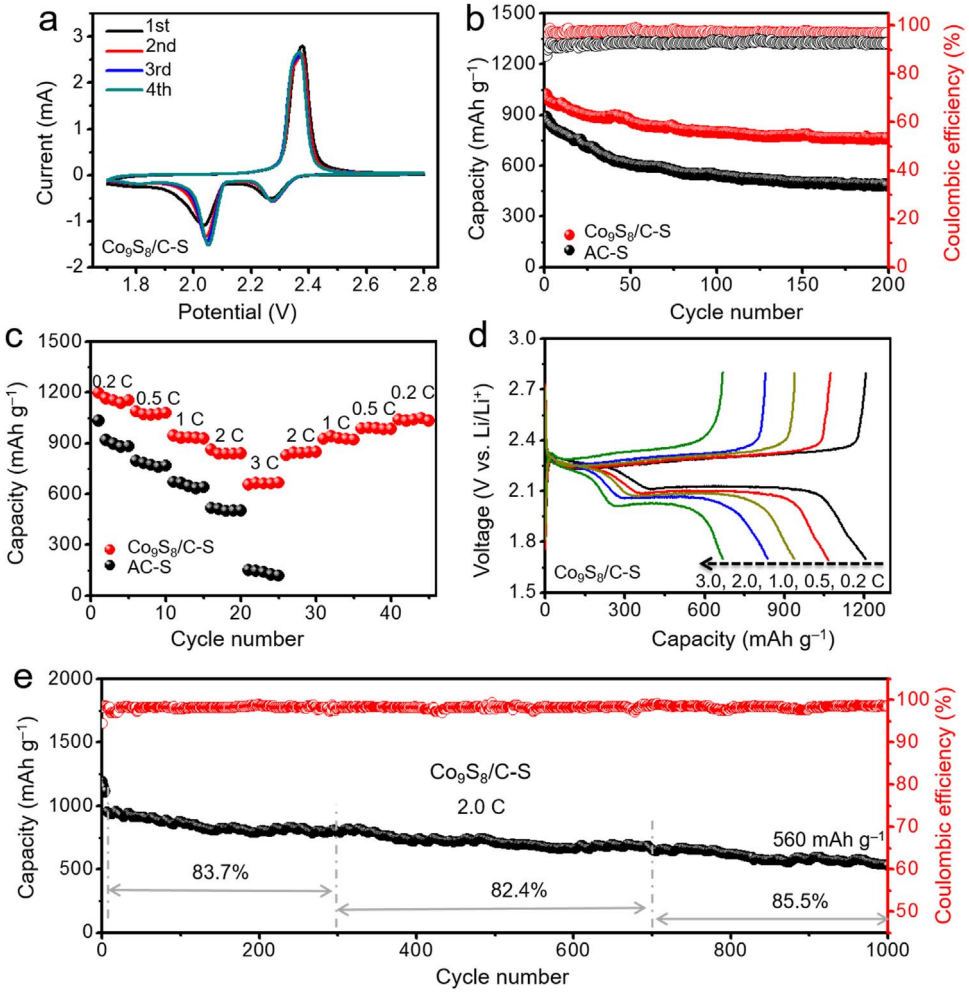

Fig. 5. (a) CV profiles of Co_9S_8/C-S cathode at a scan rate of 0.1 mV/s. (b) Cycling performances and corresponding Coulombic efficiencies of Co_9S_8/C-S and AC-S cathodes at 0.5 C. (c) Rate performances of Co_9S_8/C-S and AC-S cathodes at varied current rates. (d) Charge/discharge curves of Co_9S_8/C-S cathode at varied current rates. (e) Cycling performance of Co_9S_8/C-S cathode for 1000 cycles at a high current rate of 2.0 C.

2.8 V was measured (Fig. S10). The Co_9S_8/C electrode (without sulfur impregnation) only delivers a discharge capacity of 58 mAh g^{-1} initially and 55 mAh g^{-1} after 200 cycles, suggesting that Co_9S_8/C host has very minor contribution to the specific capacity of Co_9S_8/C-S composite cathode.

To achieve a high areal sulfur-loading is critical to meet the demand for practical applications. Therefore, we further increased the areal loading mass of sulfur to 3.0 mg cm^{-2}, and investigated the rate capability and cycling performances of these thick-film electrodes. As shown in Fig. 6a,b, the discharge capacities of high sulfur-loading Co_9S_8/C-S cathode at 0.05, 0.1, 0.2, 0.5 and 1.0 C are around 1020, 950, 890, 790, and 680 mAh g^{-1}, respectively. When the current density set back to 0.1 C, a reversible capacity of 980 mAh g^{-1} was observed, suggesting high rate performance and stability. The high sulfur-loading Co_9S_8/C-S cathode also shows excellent cycling stability at a high current of 0.5 C (2.5 mA cm^{-2}), and the discharge capacity reached 680 mAh g^{-1} after 300 cycles (Fig. 6c). This indicates a high areal capacity of 2.0 mAh cm^{-2} can be achieved with the sulfur loading of 3.0 mg cm^{-2}. Compared with other reported cathodes of sulfur/metal sulfides (Table S1 and Fig. 6d), [35–38,57,58] the Co_9S_8/C-S cathode shows relatively high rate capability, cycling performance and areal capacity.

2. Conclusions

In summary, we have designed and synthesized a novel hollow Co_9S_8/C nanopolyhedra as an efficient sulfur host for Li-S batteries. This nanostructure can efficiently prevent polysulfide shuttling by the combined chemical binding of polar Co_9S_8 nanocrystals and the spatial entrapment of carbon shells. Meanwhile, the strong interaction of Co_9S_8 with Li_2S_x species also can improve the redox reaction kinetics. In result, the Co_9S_8/C-S electrode exhibited a high specific capacity and a long cycling stability, even at high areal sulfur loading. This work provides a new and feasible route for the construction of cathode materials for high-energy and long-life Li–S batteries.

3. Experimental section

3.1. Preparation of ZIF-67 precursor nanopolyhedra

Typically, 3.2 mmol of $Co(NO_3)_2{\cdot}6H_2O$ and 9.6 mmol of 2-methylimidazole were respectively dissolved in 40 mL methanol and then mixed together rapidly under vigorously stirring. The mixture was incubated at room temperature for 24 h. The precipitate was collected by repeatedly washing with ethanol for 3 times and then dried overnight.

3.2. Synthesis of Co_9S_8/C hollow nanopolyhedra

Firstly, 60 mg of ZIF-67 precursor nanopolyhedra was dispersed into 30 mL ethanol. Then, 90 mg of thioacetamide was added into the above solution and continuously stirred for 30 min. The mixture was

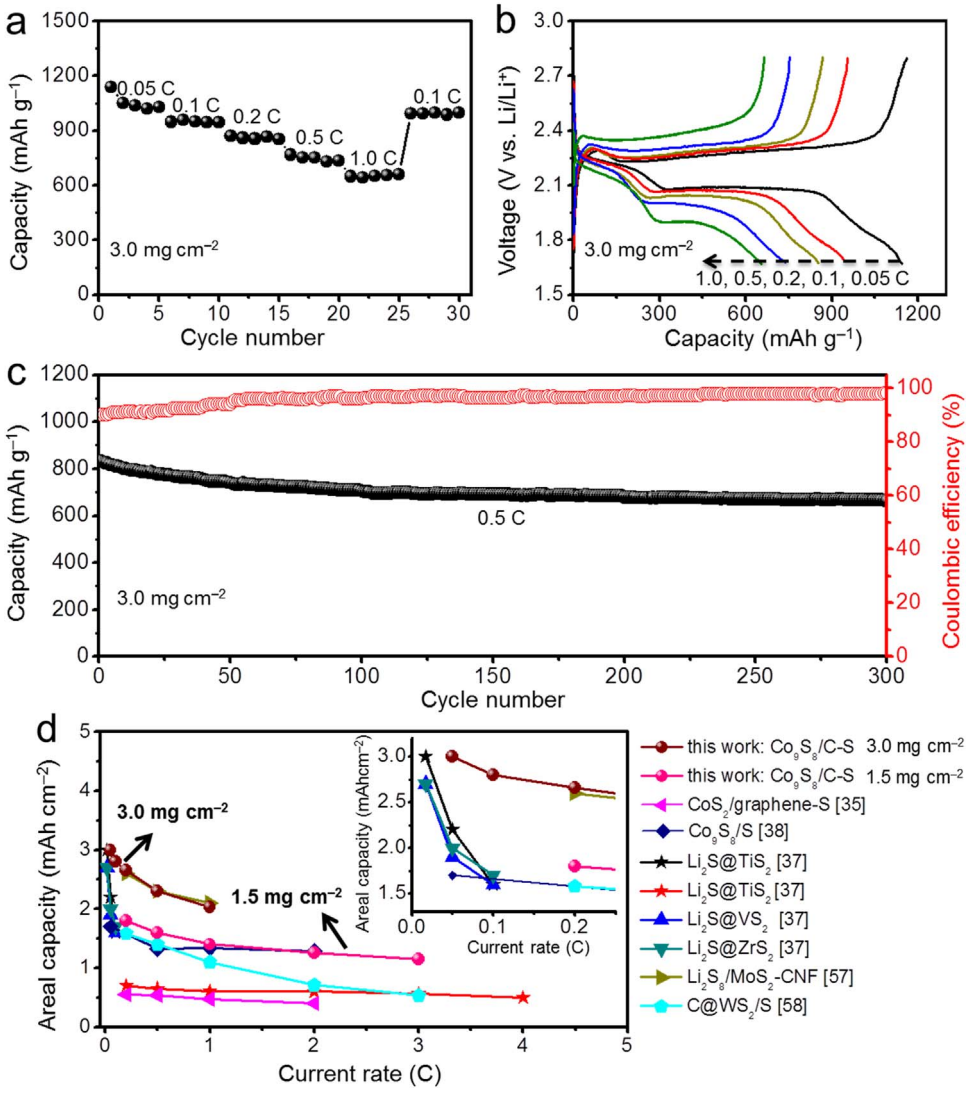

Fig. 6. (a) Discharge capacity and (b) voltage profiles of Co_9S_8/C-S cathode with a high sulfur-loading (3.0 mg cm^{-2}) at stepwise current rates from 0.05 to 1.0 C. (c) Cycle performance of high sulfur-loading Co_9S_8/C-S cathode at 0.5 C. (d) Comparisons of the rate capabilities of Co_9S_8/C-S cathodes (with different sulfur-loading) in this work with those of other reported metal sulfide/sulfur composite cathodes in previous reports [35–38,57,58].

transferred into a 50 mL Teflon-lined autoclave and maintained at 120 °C for 3 h. After cooled naturally, the product were collected and washed for 6 times with water and ethanol, respectively, and then dried under vacuum at 50 °C overnight. The product was annealed in a tube furnace at 350 °C for 2 h under N_2 atmosphere with a heating rate of 1 °C/min.

3.3. Sulfur impregnation in Co_9S_8/C hollow nanopolyhedra

Briefly, 120 mg of sulfur powder and 30 mg of Co_9S_8/C hollow nanopolyhedra with a weight ratio of 4:1 were dispersed into CS_2 and stirred at room temperature for 2 h to remove the solvent. The as-obtained mixture was ground into powder and heated at 155 °C for 6 h under N_2 atmosphere. Then, the powder was heated to 200 °C in N_2 and kept for 15 min to remove the excess sulfur particles on the surface of nanopolyhedra. The product was denoted as Co_9S_8/C-S nanopolyhedra. For comparison, the composite of commercially-available activated carbon and sulfur with the same weight ratio was also prepared by the same procedure, and named as AC-S composite.

3.4. Characterizations

The morphology and structure of the samples were analyzed by using scanning electron microscopy (SEM, HITACH S-4800, 5 kV) and transmission electron microscopy (TEM, JEOL-2100, 200 kV). Energy-dispersive X-ray spectrometer (EDX) attached on the SEM was used to analyze the compositions. The samples were characterized by X-ray diffraction (XRD) on a Shimadzu 6000 X-ray diffractometer with a Cu Kα radiation source (λ = 1.5406 Å). Nitrogen adsorption-desorption isotherms were measured through Brunauer–Emmett–Teller (BET) method with a Quantachrome Autosorb-IQ-2C-TCD-VP analyzer at liquid-nitrogen temperature. Raman spectra were collected using with a Horiba JY Evolution Raman spectrometer with an excitation laser of 532 nm wavelength. X-ray photoelectron spectra (XPS) were measured on a PHI-5000 VersaProbe X-ray photoelectron spectrometer with an Al Kα X-ray radiation. The sulfur content in the sulfur cathode composite was determined by thermogravimetric analysis (STA 449 C, NETZSCH) under N_2 with a ramp rate of 10 °C/min.

3.5. Electrochemical measurements

Typically, 80 wt% of sulfur composites, 10 wt% of acetylene black

and 10 wt% of polyvinylidene difluoride binder were dispersed in N-methyl-2-pyrrolidone. The slurry was coated on an aluminum foil and vacuum dried at 60 °C overnight to form the working electrode. The sulfur mass loading was 1.5 or 3.0 mg cm^{-2}. CR2032 coin cells were assembled in an Ar-filled glovebox with lithium metal as counter electrode, and Celgard 2400 polypropylene membrane as separator. 15 μL of 1.0 M of lithium bis(trifluoromethanesulfonyl)imide electrolyte in the mixed solvent of 1,3-dioxolane and dimethoxymethane (v/v =1:1, with 1 wt% of $LiNO_3$ additive) was added into each Li-S cell. The galvanostatic charge/discharge measurements were performed with a voltage window of 1.7–2.8 V vs. Li^+/Li using a LAND CT2001A test system. CV curves were recorded by a Chenhua CHI-760 electrochemical workstation at a sweep rate of 0.1 mV/s. EIS measurements at open-circuit potential was carried out in the range of 100 kHz to 0.01 Hz.

3.6. Computational method

The calculations were carried out using the Vienna Ab Initio Simulation Package framework of density functional theory (DFT). The exchange correlation energy was evaluated by the Perdew-Burke-Ernzehof (PBE) functional within the generalized gradient approximation (GGA). The Brillouin zone was sampled with 4×4×1 Monkhorst-Pack k-points and the plane-wave cut-off energy of 500 eV was adopted in the geometry optimization calculations to ensure the accuracy of the calculation results. All structures were optimized with the total energy and ionic force convergence criterion of 1×10^{-5} eV and 1×10^{-2} eVÅ^{-1}, respectively. In this study, the (202) surface of Co_9S_8 containing 153 atoms was chosen as the substrate. To calculate the binding energy, a periodic three-layered supercell of Co_9S_8 was employed. The adsorption energy (E_a) of Li_nS_x with Co_9S_8 is calculated by the equation:

$$E_a = E_{(Co_9S_8)} + E_{(Li_nS_x)} - E_{(Co_9S_8/Li_nS_x)} (\mathrm{n} = 0, \mathrm{x} = 8 \text{ or } \mathrm{n} = 2, \mathrm{x} = 1, 2, 4, 6, 8)$$

where $E_{(Co9S8)}$, $E_{(LinSx)}$ and $E_{(Co9S8/LinSx)}$ are the total energy of the substrate, Li_nS_x and Li_nS_x-substrate, respectively. According to this equation, the more negative E_a value indicates the more stronger binding interaction between Li_nS_x and the surface of Co_9S_8.

3.7. Experimental comparisons of Li_2S_4 adsorption capabilities

All operations were completed in an Ar-filled glove box. Firstly, sulfur powder and lithium superhydride ($LiEt_3BH$) with a molar ratio of 2.75:1 was added into anhydrous tetrahydrofuran (THF) with continuous stirring at room temperature for 1 h. The resulting Li_2S_4 product was collected by washing with toluene, centrifugation and vacuum dry. For the visual comparison of polysulfide absorption ability, 50 mg of Co_9S_8/C powder or activated carbon were soaked in 2 mL of Li_2S_4 solution (0.2 wt% in mixed DOL/DME solvents with a volume ratio of 1:1). To further compare the polysulfide confinement ability of Co_9S_8/C-S and AC-S cathodes, the electrodes were cycled in coin cells for 200 times at 0.5 C and taken out from coin cells, and then soaked in the DOL/DME solution of Li_2S_4.

Acknowledgements

This work was supported by National Materials Genome Project (2016YFB0700600), National 973 Basic Research Program (2015CB659300), National Natural Science Foundation of China (21403105, 21573108), China Postdoctoral Science Foundation (2015M580413, 2015M581769), Natural Science Foundation for Young Scholars of Jiangsu Province (BK20150583, BK20160647), Fundamental Research Funds for the Central Universities and a project funded by the Priority Academic Program Development (PAPD) of Jiangsu Higher Education Institutions.

Appendix A. Supporting information

Supplementary data associated with this article can be found in the online version at doi:10.1016/j.nanoen.2017.05.064.

References

[1] J.B. Goodenough, Chem. Soc. Rev. 46 (2013) 1053–1061.
[2] J.W. Choi, D. Aurbach, Nat. Rev. Mater. 1 (2016) 16013.
[3] Y. Tang, Y. Zhang, W. Li, B. Ma, X. Chen, Chem. Soc. Rev. 44 (2015) 5926–5940.
[4] P.G. Bruce, S.A. Freunberger, L.J. Hardwick, J.M. Tarascon, Nat. Mater. 11 (2011) 19–29.
[5] L. Fei, X. Li, W. Bi, Z. Zhuo, W. Wei, L. Sun, W. Lu, X. Wu, K. Xie, C. Wu, H.L.W. Chan, Y. Wang, Adv. Mater. 27 (2015) 5936–5942.
[6] Y.R. Wang, R.P. Chen, T. Chen, H.L. Lv, G.Y. Zhu, L.B. Ma, C.X. Wang, Z. Jin, J. Liu, Energy Storage Mater. 4 (2016) 103–129.
[7] R. Xu, J. Lu, K. Amine, Adv. Energy Mater. 5 (2015) 1500408.
[8] Y.X. Yin, S. Xin, Y.G. Guo, L.J. Wan, Angew. Chem. Int. Ed. 52 (2013) 13186–13200.
[9] A. Manthiram, Y. Fu, S.H. Chung, C. Zu, Y.S. Su, Chem. Rev. 114 (2014) 11751–11787.
[10] X. Liu, J.Q. Huang, Q. Zhang, L.Q. Mai, Adv. Mater. 1601759 (2017).
[11] C. Lin, C.J. Niu, X. Xu, K. Li, Z., Y. Cai, Y.L. Zhang, X.P. Wang, L.B. Qu, Y.X. Xu, L.Q. Mai, Phys. Chem. Chem. Phys. 18 (2016) 22146–22153.
[12] G.M. Zhou, E. Paek, G.S. Hwang, A. Manthiram, Adv. Energy Mater. 6 (2016) 1501355.
[13] L. Suo, Y.S. Hu, H. Li, M. Armand, L. Chen, Nat. Commun. 4 (2013) 1481.
[14] G.M. Zhou, S.F. Pei, L. Li, D.W. Wang, S.G. Wang, K. Huang, L.C. Yin, F. Li, H.M. Cheng, Adv. Mater. 26 (2014) 625–631.
[15] X. Ji, S. Evers, R. Black, L.F. Nazar, Nat. Commun. 2 (2011) 325.
[16] X. Ji, K.T. Lee, L.F. Nazar, Nat. Mater. 8 (2009) 500–506.
[17] S. Rehman, S. Guo, Y. Hou, Adv. Mater. 28 (2016) 3167–3172.
[18] N. Jayaprakash, J. Shen, S.S. Moganty, A. Corona, L.A. Archer, Angew. Chem. Int. Ed. 50 (2011) 5904–5908.
[19] C.F. Zhang, H.B. Wu, C.Z. Yuan, Z.P. Guo, X.W. Lou, Angew. Chem. Int. Ed. 51 (2012) 9592–9595.
[20] G. He, S. Evers, X. Liang, M. Cuisinier, A. Garsuch, L.F. Nazar, ACS Nano 7 (2013) 10920–10930.
[21] Z.Y. Wang, Y.F. Dong, H.J. Li, Z.B. Zhao, H.B. Wu, C. Hao, S.H. Liu, J.S. Qiu, X.W. Lou, Nat. Commun. 5 (2014) 5002.
[22] M.Q. Zhao, Q. Zhang, J.Q. Huang, G.L. Tian, J.Q. Nie, H.J. Peng, F. Wei, Nat. Commun. 5 (2014) 3410.
[23] H.L. Wang, Y. Yang, Y.Y. Liang, J.T. Robinson, Y.G. Li, A. Jackson, Y. Cui, H.J. Dai, Nano Lett. 11 (2011) 2644–2647.
[24] G.M. Zhou, D.W. Wang, F. Li, P.X. Hou, L.C. Yin, C. Liu, G.Q. Lu, I.R. Gentle, H.M. Cheng, Energy Environ. Sci. 5 (2012) 8901–8906.
[25] Y. Fu, Y.S. Su, A. Manthiram, Angew. Chem. Int. Ed. 125 (2013) 7068–7073.
[26] S. Zhang, S. Tsuzuki, K. Ueno, K. Dokko, M. Watanabe, Angew. Chem. Int. Ed. 54 (2015) 1302–1306.
[27] F. Pei, T.H. An, J. Zhang, X.J. Zhao, X.L. Fang, M.S. Zheng, Q.F. Dong, N.F. Zheng, Adv. Energy Mater. 6 (2016) 1502539.
[28] Y.L. Ding, P. Kopold, K. Hahn, P.A. van Aken, J. Maier, Y. Yu, Adv. Funct. Mater. 26 (2016) 1112–1119.
[29] C. Tang, Q. Zhang, M.Q. Zhao, J.Q. Huang, X.B. Cheng, G.L. Tian, H.J. Peng, F. Wei, Adv. Mater. 26 (2014) 6100–6105.
[30] X. Liang, C. Hart, Q. Pang, A. Garsuch, T. Weiss, L.F. Nazar, Nat. Commun. 6 (2015) 5682.
[31] X.L. Wang, G. Li, J.D. Li, Y.N. Zhang, A. Wook, A.P. Yu, Z.W. Chen, Energy Environ. Sci. 9 (2016) 2533–2538.
[32] Z. Liang, G.Y. Zheng, W.Y. Li, Z.W. She, H.B. Yao, K. Yan, D.S. Kong, Y. Cui, ACS Nano 8 (2014) 5249–5256.
[33] Q. Pang, D. Kundu, M. Cuisinier, L.F. Nazar, Nat. Commun. 5 (2014) 4759.
[34] X.T. Tao, J.G. Wang, Z.G. Ying, Q.X. Cai, G.Y. Zheng, Y.P. Gan, H. Huang, Y. Xia, C. Liang, W.K. Zhang, Y. Cui, Nano Lett. 14 (2014) 5288–5294.
[35] Z. Li, J.T. Zhang, B.Y. Guan, D. Wang, L.-M. Liu, X.W. Lou, Nat. Commun. 7 (2016) 13065.
[36] Z. Yuan, H.J. Peng, T.Z. Hou, J.Q. Huang, C.M. Chen, D.W. Wang, X.B. Cheng, F. Wei, Q. Zhang, Nano Lett. 16 (2016) 519–527.
[37] Q. Pang, D. Kundu, L.F. Nazar, Mater. Horiz. 3 (2016) 130–136.
[38] Z.W. Seh, J.H. Yu, W.Y. Li, P.-C. Hsu, H.T. Wang, Y.M. Sun, H.B. Yao, Q.F. Zhang, Y. Cui, Nat. Commun. 5 (2014) 5017.
[39] S.S. Zhang, D.T. Tran, J. Mater. Chem. A 4 (2016) 4371–4374.
[40] Z.M. Cui, C.X. Zu, W.D. Zhou, A. Manthiram, J.B. Goodenough, Adv. Mater. 28 (2016) 6926–6931.
[41] X. Liang, A. Garsuch, L.F. Nazar, Angew. Chem. Int. Ed. 54 (2015) 3907–3911.
[42] H.J. Peng, G. Zhang, X. Chen, Z.W. Zhang, W.T. Xu, J.Q. Huang, Q. Zhang, Angew. Chem. Int. Ed. 55 (2016) 12990–12995.
[43] X. Liang, Y. Rangom, C.Y. Kwok, Q. Pang, L.F. Nazar, Adv. Mater. 29 (2017) 1603040.
[44] H. Li, Y.H. Gao, Y.D. Shao, Y.T. Su, X.W. Wang, Nano Lett. 15 (2015) 6689–6695.
[45] R.C. Hoodless, R.B. Moyes, P.B. Wells, Catal. Today 114 (2006) 377–382.
[46] J. Liu, C. Wu, D.D. Xiao, P. Kopold, L. Gu, P.A. van Aken, J. Maier, Y. Yu, Small 12 (2016) 2354–2364.
[47] J. Jiang, J.H. Zhu, W. Ai, X.L. Wang, Y.L. Wang, C.J. Zou, W. Huang, T. Yu, Nat.

Commun. 6 (2015) 8622.
[48] D.B. Yu, L. Ge, B. Wu, L. Wu, H.T. Wang, T.W. Xu, J. Mater. Chem. A 3 (2015) 16688–16694.
[49] H. Hu, B.Y. Guan, B.Y. Xia, X.W. Lou, J. Am. Chem. Soc. 137 (2015) 5590–5595.
[50] H. Hu, J.T. Zhang, B.Y. Guan, X.W. Lou, Angew. Chem. Int. Ed. 55 (2016) 9514–9518.
[51] Y.D. Yin, R.M. Rioux, C.K. Erdonmez, S. Hughes, G.A. Somorjai, A.P. Alivisatos, Science 304 (2004) 711–714.
[52] Z. Wang, L. Pan, H. Hu, S. Zhao, CrystEngComm 12 (2010) 1899–1904.
[53] X. Chen, H.J. Peng, R. Zhang, T.Z. Hou, J.Q. Huang, B. Li, Q. Zhang, ACS Energy Lett. 2 (2017) 795–801.
[54] H.J. Zhou, Z., W. Zhang, J.Q. Huang, G. Zhang, J. Xie, W.T. Xu, J.L. Shi, X. Chen, X.B. Cheng, Q. Zhang, Adv. Mater. 28 (2016) 9551–9558.
[55] Y.X. Zhou, H.B. Yao, Y. Wang, H.L. Liu, M.R. Gao, P.-K. Shen, S.H. Yu, Chem. -Eur. J. 16 (2010) 12000–12007.
[56] X.L. Wang, G. Li, M.H. Seo, F.M. Hassan, M.A. Hoque, Z.W. Chen, Adv. Energy Mater. 5 (2015) 1501106.
[57] H.T. Wang, Q.F. Zhang, H.B. Yao, Z. Liang, H.-W. Lee, P.-C. Hsu, G.Y. Zheng, Y. Cui, Nano Lett. 14 (2014) 7138–7144.
[58] T.Y. Lei, W. Chen, J.W. Huang, C.Y. Yan, H.X. Sun, C. Wang, W.L. Zhang, Y.R. Li, J. Xiong, Adv. Energy Mater. 7 (2016) 1601843.

Dr. Tao Chen received his Ph.D. degree in Chemical Engineering and Technology under supervision of Prof. Jiajun Fu from Nanjing University of Science and Technology in June 2015. He is currently a postdoctoral researcher in the group of Prof. Zhong Jin and Prof. Jie Liu at Nanjing University. His current research focuses on the design and synthesis of nanostructured electrode materials for rechargeable batteries.

Lianbo Ma received his M.S. degree in Applied Chemistry from Jiangsu University, PR China (2015). He is now pursing his Ph.D. degree under the supervision of Prof. Zhong Jin and Jie Liu in School of Chemistry and Chemical Engineering, Nanjing University, P.R. China. His main interest is the design and fabrication nanomaterials for photoelectric conversion.

Baorui Cheng entered School of Chemistry and Chemical Engineering, Nanjing University in 2013. He majors in chemistry and currently works as an assistant of Dr. Tao Chen in the group of Prof. Zhong Jin. His current research focuses on preparation of MOFs-based functional materials.

Renpeng Chen has graduated from the Northeastern University (China) since 2014. Now, he is pursuing his M.S. degree under the guidance of Prof. Zhong Jin in School of Chemistry and Chemical Engineering at Nanjing University. His research interest is focused on the synthesis of alloy materials for lithium-ion batteries.

Yi Hu received his B.S. degree in Chemistry from Sichuan University in 2014. He is now pursuing his Ph.D. degree under the supervision of Prof. Zhong Jin in School of Chemistry and Chemical Engineering at Nanjing University. His research interests reside in two-dimensional nanomaterials for electrochemical energy storage and photoelectric conversion.

Guoyin Zhu obtained his M.S. degree from Nanjing University of Posts & Telecommunications in 2014. Currently, he is pursuing his Ph.D. degree under the supervision of Prof. Zhong Jin and Jie Liu at Nanjing University. His research is mainly focused on the synthesis of carbonaceous nanomaterials, and their application for energy conversion and storage devices.

Yanrong Wang received her master degree in physical chemistry under the supervision of Professor Yong Hu in College of Chemistry and life sciences at Zhejiang Normal University in 2015. She is now pursuing her Ph.D. degree under the supervision of Prof. Zhong Jin and Jie Liu in School of Chemistry and Chemical Engineering at Nanjing University. Her current research interest is the design of new type of battery.

Dr. Jia Liang received his Ph.D. in the Key Laboratory for Physics and Chemistry of Nanodevices from Peking University in 2015, under the guidance of Prof. Gengmin Zhang. He joined Prof. Jun Lou's research group in Rice University as a visiting student in 2014. He is currently an assistant researcher in the group directed by Prof. Zhong Jin and Jie Liu at Nanjing University. His main research interest is synthesis of energy nanomaterials and their applications in solar cells, catalyses, and flow batteries.

Dr. Zuoxiu Tie received her B.S. (2004) degree and Ph.D. (2010) from Nanjing University. She is currently a research associate in the group of Prof. Zhong Jin. Her current research interest focuses on carbonaceous nanomaterials for energy conversion and storage devices.

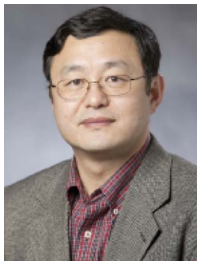

Prof. Jie Liu is currently the George B. Geller Professor of Chemistry at Duke University and an adjunct professor of "Thousands Talents" Program at Nanjing University. He earned a B.S. from Shandong University in 1987 and a Ph.D. from Harvard University in 1996. His research interests include the synthesis and chemical functionalization of nanomaterials, nanoelectronic devices, scanning probe microscopy, and carbon nanomaterials. Prof. Liu is a Fellow of the AAAS, APS and RSC.

Prof. Zhong Jin received his B.S. (2003) and Ph.D. (2008) in chemistry from Peking University. He worked as a postdoctoral scholar at Rice University and Massachusetts Institute of Technology. Now he is a professor in School of Chemistry and Chemical Engineering at Nanjing University. He leads a research group working on advanced materials and devices for energy conversion and storage.